A Model-Based Computationally Efficient Method for On-Line Detection of Chatter in Milling

Lei Ma

Shreyes N. Melkote

George W. Woodruff School of Mechanical Engineering, Georgia Institute of Technology, Atlanta, GA 30332

James B. Castle

The Boeing Company, Boeing Research and Technology, St. Louis, MO 63166

This paper presents a model-based computationally efficient method for detecting milling chatter in its incipient stages and for chatter frequency estimation by monitoring the cutting force signals. Based on a complex exponentials model for the dynamic chip thickness, the chip regeneration effect is amplified and isolated from the cutting force signal for early chatter detection. The proposed method is independent of the cutting conditions. With the aid of a one tap adaptive filter, the method is shown to be capable of distinguishing between chatter and the dynamic transients in the cutting forces arising from sudden changes in workpiece geometry and tool entry/exit. To facilitate chatter suppression once the onset of chatter is detected, a time domain algorithm is proposed so that the dominant chatter frequency can be accurately determined without using computationally expensive frequency domain transforms such as the Fourier transform. The proposed method is experimentally validated. [DOI: 10.1115/1.4023716]

1 Introduction

Chatter imposes a major limitation on the productivity of milling processes and results in poor part quality, accelerated tool wear, and shortened spindle life. Milling chatter has been theoretically studied by many researchers including Altintas and his coworkers [1,2], Stepan and Insperger [3,4], and Davies et al. [5]. Given cutting conditions, tool/workpiece material models, and structural dynamics model of the tool/workpiece/fixture/machine tool system, the occurrence of chatter can be predicted with reasonable accuracy. However, unstable cutting may still occur under the "chatter-free" cutting conditions because process related uncertainties such as material inhomogeneity, nonlinearity between the cutting force and chip thickness [6], and tool wear are usually ignored in milling chatter theory. The lack of reliable structural dynamics models also limits the usefulness of milling chatter theory in industrial applications. Therefore, on-line detection and suppression of chatter in milling via process monitoring is still highly desirable, especially for high added value parts.

Prior work on chatter detection generally employs three types of signal processing methods, including: (1) transform domain analysis such as the Fourier transform, power spectrum, the short time Fourier transform (STFT) [7–19], and wavelet transform [20–27], (2) time domain modeling and analysis [28–46], and (3) pattern recognition [47] and classification algorithms such as artificial neutral networks [25,48–54], fuzzy logic [55], the hidden Markov model [56,57], support vector machine [22,57] and the index based reasoner [58].

The classical Fourier transform and power spectrum are not suited for on-line chatter detection. The Fourier transform of the chatter signal can reveal the existence of chatter frequency but not its "time of arrival" due to the infinite support of the eigenfunctions used in the Fourier transform. Linear time-frequency analysis methods such as the STFT and wavelet transform have been extensively studied by researchers for chatter detection. The STFT suffers from the inherent limitation that good time domain and frequency domain resolution cannot be simultaneously achieved. The frequency resolution of the STFT was identified as the primary performance bottleneck of the classical audio signal based chatter detection and suppression system developed in Ref. [11]. Wavelet transform achieves a compromise between time domain resolution and frequency domain resolution. However, the resolution in the high frequency band is inadequate. When the chatter frequency is not known *a priori*, it is difficult to determine the number of levels of decomposition needed and which level(s) is(are) sensitive to the transition from chatter-free cutting to unstable cutting. The choice of the mother wavelet function can also have a major impact on the performance of the algorithm, which further complicates the application of wavelet-based methods. Finally, wavelet transform based algorithms for chatter detection proposed in the literature [20–27] cannot accurately pinpoint the dominant chatter frequency.

Chatter detection methods based on pattern recognition and classification algorithms suffer from the drawback that extensive training is needed before they can function. Also, decisions made by the classification algorithms are not physically meaningful and some of the methods are unable to identify the chatter frequency [22,58].

Time series features such as coherence [45], coarse-grain entropy rate [31], permutation entropy [59], singular values of the Toeplitz matrix of the third order cumulants of acceleration measurements [32], and statistical modeling [36] have been used to recognize chatter in turning. However, the existence of forced vibrations at the tooth passing frequency and its harmonics in milling limits the applicability of these methods.

Descriptive statistical analysis of the cutting force [34] and audio signal [35] was used to detect chatter in milling. The assumption made in Ref. [34] that the cutting force approaches a Gaussian distribution when chatter occurs is questionable. The once-per-revolution sampling method proposed in Ref. [35] is computationally very efficient but sensitive to the measurement errors and various transient events in the cutting process. Furthermore, most time series analysis methods [28,29,31,32,34–37,39,40] cannot identify the chatter frequency.

In the early work by Braun [7] the phase information of the complex demodulated acceleration signal acquired from turning was found to be sensitive to the state transition of the cutting process dynamics. The time domain method obviates the difficulties associated with frequency domain methods when nonstationary signals are concerned. However, the phase computed using a regular arctangent function is, in general, discontinuous and unwrapping of the phase can be difficult [60].

Choi and Shin [20] proposed a cutting condition independent and computationally inexpensive chatter index that is inversely

Contributed by the Manufacturing Engineering Division of ASME for publication in the Journal of Manufacturing Science and Engineering. Manuscript received April 2, 2012; final manuscript received October 29, 2012; published online May 24, 2013. Assoc. Editor: Tony Schmitz.

related to the dimension of the cutting process dynamics. However, it is not clear whether the reduction in dimension occurs before or after chatter is fully developed.

Al-Regib and Ni [28] suggested using the ratio of the high-frequency band energy to the total energy in a signal as an indicator of chatter. While this normalized index is process and cutting conditions independent, its usefulness in milling is questionable because at the incipient stages of chatter, the energy around the chatter frequencies is still smaller than the energy around the spindle speed related frequencies. Additionally, it is hard to define what a high frequency band is when the chatter frequencies are unknown.

van Dijk et al. [46] proposed an interesting method which decomposes the signal acquired from a spindle mounted accelerometer into two parts: a periodic part due to rigid body rotation and a perturbation part due to tool deflection and chip regeneration. The former part was modeled as a moving average (MA) process and the latter as an autoregressive (AR) process, which is recursively estimated and used for chatter detection. However, the assignment of an AR model to the chip regeneration part of the signal is not supported by cutting force models. In addition, significant estimation errors may occur if the order of the AR model is not chosen appropriately.

The multisensor and multi-index chatter detection approach developed by Kuljanic et al. [8,50] effectively improves the reliability of the chatter detection system and reduces the false alarm rate. However, the method is computationally expensive and significant instrumentation effort is needed.

Besides, since most of the aforementioned methods are only validated in simple straight line cutting experiments, it is unclear whether they would still work if the toolpath is curvilinear or if the workpiece geometry has discontinuities (such as holes, slots, pockets, etc.) that can cause transient dynamic behaviors during cutting.

In this paper, we present a novel cutting-force-based time domain algorithm for incipient detection of milling chatter and for estimating the dominant chatter frequency. The chatter detection algorithm is an extension of the tool breakage detection algorithm proposed by Altintas [61]. It is shown that the proposed algorithm is capable of detecting the onset of chatter and distinguishing between chatter and workpiece geometry induced transients in the cutting force signal. The chatter frequency estimation algorithm originates from the spectrum estimation of a complex exponentials signal embedded in white noise and is shown to be as accurate as and computationally more efficient than Fourier transform based methods. In the following sections, the proposed methodology is presented with experimental verification and discussion of the computational complexity and conclusions.

2 Methodology

2.1 Complex Exponentials Cutting Force Model. The cutting force is chosen as the source signal for chatter detection because of the availability of well-established mechanistic models for milling. As established in Ref. [1], with the absence of runout, the instantaneous tangential force f_j^t and the radial force f_j^r acting on tooth j in the cut are given by (see Fig. 1)

$$\begin{aligned} f_j^t &= g(\phi_j(t))K_s a[s_t \sin(\phi_j(t)-\pi) + A_j^p \sin(\omega_c t + \psi_j^p) \\ &\quad - A_j^c \sin(\omega_c t + \psi_j^c)] \\ f_j^r &= K_r f_j^t \end{aligned} \tag{1}$$

where K_s is the specific cutting force coefficient, a is the axial depth of the cut, s_t is the feed per tooth, $\phi_j(t)$ is the instantaneous angular position of tooth j, K_r is the ratio of the radial force to the tangential force, A_j^p and A_j^c are the amplitudes of the chip regeneration waviness in the previous and current tooth passes, respectively, and ψ_j^p and ψ_j^c denote the phases of the chip regeneration

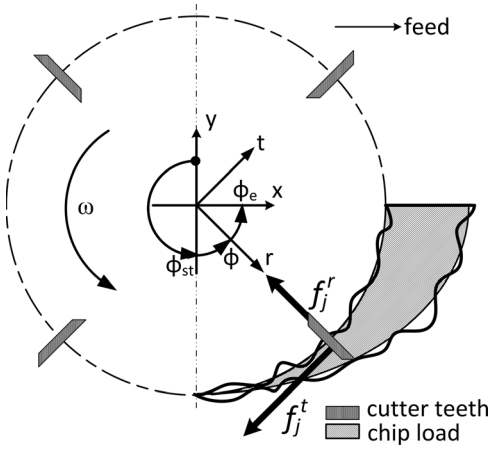

Fig. 1 Chip regeneration in milling

waviness in the previous and current tooth pass, respectively, ω_c is the chip regeneration frequency or chatter frequency, and $g(\phi)$ is a rectangular window function that simulates the interrupted cutting behavior and is defined as

$$g(\phi) = \begin{cases} 1 & \phi_{st} < \phi < \phi_e \\ 0 & \text{otherwise} \end{cases} \tag{2}$$

where ϕ_{st} and ϕ_e are the angular positions of tooth entry and exit, respectively. Resolving f_j^t and f_j^r into the workpiece coordinate system (x-y), we have

$$\begin{aligned} f_j^x &= f_j^t \cos\phi_j + f_j^r \sin\phi_j \\ f_j^y &= f_j^t \sin\phi_j - f_j^r \cos\phi_j \end{aligned} \tag{3}$$

The total cutting force is simply the summation of the resolved forces over all teeth engaged in cutting

$$F_x(t) = \sum_{j=1}^{z} f_j^x, \quad F_y(t) = \sum_{j=1}^{z} f_j^y \tag{4}$$

It can be shown that with no chip regeneration, i.e., $A_j^p = A_j^c = 0$, F_x and F_y are periodic functions with a period of

$$\tau_T = 2\pi/z\omega \tag{5}$$

where z is the number of cutter teeth, ω is the angular speed of the tool (also known as the spindle frequency), τ_T denotes the tooth period, $\tau = z\tau_T$ represents the spindle period, and $\omega_T = 2\pi/\tau_T$ is the tooth passing frequency. Due to the periodic rectangular window functions $g(\phi_j)$, the Fourier series expansion of $F(t)$ (which can be $F_x(t)$, $F_y(t)$ or a functional combination of the two) consists of an infinite number of higher order harmonics of the tooth passing frequency and the chip regeneration frequency [4]

$$F(t) = \sum_{k=-\infty}^{\infty} F_k e^{jk\omega_T t} + \sum_{k=-\infty}^{\infty} [C_k^+ e^{j(\omega_c + k\omega_T)t} + C_k^- e^{j(-\omega_c - k\omega_T)t}] \tag{6}$$

where ω_c is still the chip regeneration frequency and F_k, $C_k{}^+$, and C_k^- denote the complex amplitudes of the corresponding harmonics. Since $F(t)$ is a real signal, it follows

$$F_k = (F_{-k})^*, \; C_k^+ = (C_k^-)^* \tag{7}$$

where * denotes the complex conjugate operator. Since the energy contained in the cutting force signal is finite, only a limited

number of the higher order harmonics are significant and the rest of them can be safely dropped. If we consider a measured cutting force signal $\hat{F}(t)$, a random disturbance needs to be added to account for the various random processes also present in the actual process, e.g., material inhomogeneities, noise in the measurement system, etc. In light of the central limit theorem, the aggregation of all of these random processes can be modeled as a white Gaussian noise. Therefore, the Fourier series expansion of $\hat{F}(t)$ can be established as

$$\hat{F}(t) \approx \sum_{k=-N_1}^{N_1} F_k e^{jk\omega_T t} + \sum_{k=-N_2}^{N_2} [C_k^+ e^{j(\omega_c + k\omega_T)t} + C_k^- e^{j(-\omega_c - k\omega_T)t}] + w(t) \tag{8}$$

where $w(t)$ is the additive Gaussian white noise and N_1 and N_2 determine the number of significant harmonics of the tooth passing frequency and the chip regeneration frequency, respectively. The insight provided by Eq. (8) is that $\hat{F}(t)$ consists of three parts: a periodic part due to the rigid body motion of the cutting tool and interrupted cutting, an aperiodic chip regeneration part due to instantaneous deflections of the tool/workpiece and an unknown stochastic disturbance due to material inhomogeneity, measurement system noise, etc. When the cutting process is stable, the cutting force is dominated by the periodic part. During the transition from chatter-free cutting to unstable cutting, the chip regeneration part starts to grow and eventually dominates the cutting force signal after chatter is fully developed.

2.2 Chatter Detection Algorithm. The proposed chatter detection algorithm is based on the complex exponentials model given in Eq. (8) and contains four steps aimed at isolating and amplifying the chip regeneration part and compensating for the transients introduced by tool entry/exit, workpiece geometry variations, and other nonstationary events that may occur during milling. These four steps are described next.

2.2.1 Differentiation. Since the chip regeneration frequency is usually higher than the tooth passing frequency, the force signal is first differentiated with respect to time to amplify the high frequency content in the force signal. It is clear from Eq. (8) that differentiation usually causes the chip regeneration frequency content to be amplified by a larger ratio than the tooth passing frequency. Note that after differentiation, the periodic part still has the same period as before. This step is summarized as follows:

$$df(t) = \frac{d}{dt}\hat{F}(t) \tag{9}$$

To prevent the ultrahigh frequency content in $\hat{F}(t)$ from being inappropriately amplified by the differentiation, the frequency band above the highest possible chatter frequency is attenuated before differentiation. As suggested in Ref. [9], chatter vibrations range in frequencies from 200 Hz to as high as 4000 Hz. Therefore, the cut-off frequency of the anti-aliasing filter was set to 5000 Hz in this work so that the ultrahigh frequencies in the source signal will not present any problem during differentiation.

Since the cutting force signal is almost always discretized, the differentiation operation is approximated by finite order differences. Three finite impulse response (FIR) filters (1st, 2nd, and and 3rd order) that approximate the ideal differentiator in the least squares sense are designed and their frequency responses are shown in Fig. 2. It can be seen that all three FIR filters are very similar in performance in the 0 to 0.2 Hz range. Beyond 0.2 Hz, the 1st order FIR filter outperforms the others. Therefore, the 1st order FIR filter, which is essentially the first order difference, is used in this study

$$df(n) = \hat{F}(n) - \hat{F}(n-1) \tag{10}$$

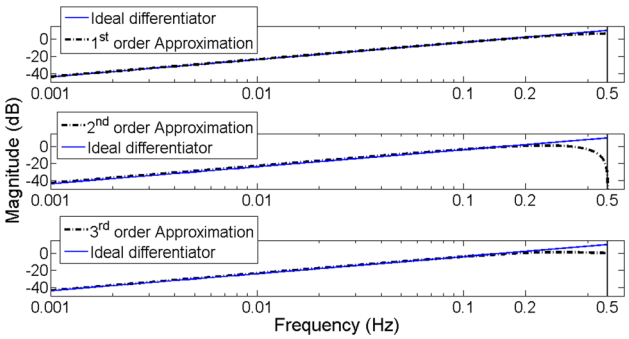

Fig. 2 Ideal differentiator and its finite order approximations

2.2.2 Spindle Period Averaging. Because the periodic part of the cutting force signal is due to the tooth period, it can be isolated from the chip regeneration content, which is due to the instantaneous deflection of the tool and/or the workpiece. In order to make the chip regeneration part of the signal stand out, the tooth passing frequency and its harmonics need to be removed. It is proposed in Ref. [55] to remove each harmonic with a notch filter, which is computationally very expensive. In addition, the number of notch filters needed is difficult to determine. In this work, the removal of the periodic content in the measured force signal is achieved in the time domain by integrating the measured cutting force signal over its smallest period, which, in theory, is τ_T. However, due to cutter runout, the cutting force signal usually contains the spindle frequency and its harmonics. Accordingly, the smallest period of the periodic part in the cutting force signal is τ. Therefore, $df(t)$ is integrated over the spindle period instead. To magnify the signal-to-noise ratio, the integration is performed on the second power of $df(t)$ as follows:

$$x_k = \int_{(k-1)\tau}^{k\tau} df(t)^2 dt \tag{11}$$

Note that the outcome of this step is a time series x_k corresponding to the spindle period k. In this step, the periodic part in $\hat{F}(t)$ results in a global DC trend in x_k, while the chip regeneration part and the stochastic disturbance may vary slightly from one spindle period to the next, leading to local variations around the DC trend. During stable cutting, the amplitudes of the chip regeneration part and the stochastic disturbance are much smaller than that of the periodic part. Therefore, the local variation in x_k around the DC trend is small in stable cutting.

When dealing with discretized $df(t)$, the integration in Eq. (11) is approximated by summation over the spindle period and can be recursively implemented in time. Per convention, x_k is treated as a time series sampled at the unit frequency.

2.2.3 One Tap Adaptive Filtering. In stable cutting, if the chip load is exactly the same from one spindle period to the next, we expect the DC trend in x_k to be time invariant, or

$$x_{k+1} = x_k + a_k \tag{12}$$

where a_k is a normally and independently distributed random process that is attributed to the stochastic disturbance and the chip regeneration part from one spindle period to the next. Equation (12) describes a first order autoregressive (AR) process, which is usually referred to as the random walk process. However, the AR (1) model is not valid when the chip load varies with time; for example, during tool entry/exit or when the tool passes through an existing geometric feature in the workpiece, e.g., a hole [61]. Under these circumstances, the time varying AR (1) model in Eq. (13) is more appropriate

$$a_k = x_{k+1} - \beta_k x_k \tag{13}$$

where β_k is the time varying AR (1) coefficient. In macro and mesoscale milling, the tool feed is small compared to the tool diameter and, in general, the size of the preexisting workpiece geometric features. Therefore, the preexisting geometric features cause the chip load to vary only slightly from one spindle period to the next and the global DC trend in x_k to vary slowly and smoothly over the time. This global variation is different in behavior from the small local variations in x_k caused by the stochastic disturbance $w(t)$ and the chip regeneration content, as illustrated in Fig. 3.

Equation (13) can be implemented as a one-step predictor with a time varying tap weight β_k, which can be adaptively updated in each spindle period with the latest data x_{k+1} using the recursive least squares (RLS) algorithm [62]. One recursion of the RLS algorithm is given here for completeness

$$\begin{aligned} a_k &= x_{k+1} - \beta_k x_k, \quad & K &= P_k x_k/(\lambda + x_k P_k x_k) \\ \beta_{k+1} &= \beta_k + K a_k, \quad & P_{k+1} &= (1 - K x_k) P_k/\lambda \end{aligned} \tag{14}$$

where λ is the forgetting factor controlling how many past data points to take into account for predicting the next sample, P_k is the inverse of the autocorrelation matrix of x_k, and K is the Kalman gain. Note that a_k is known as the *a priori* error in adaptive filtering literature and the innovation in the Kalman filter literature. Since a one tap adaptive filter is adopted here, P_k and K are both scalars. For the sake of implementation, Eq. (14) can be rearranged as follows:

$$\begin{aligned} a_k &= x_{k+1} - \beta_k x_k, \quad & K &= P_k x_k/(\lambda + (P_k x_k) x_k) \\ \beta_{k+1} &= \beta_k + K a_k, \quad & P_{k+1} &= P_k/(\lambda + (P_k x_k) x_k) \end{aligned} \tag{15}$$

When the cutting process is stable, the RLS filter enables the slow and smooth variation in the global trend in x_k due to the time varying chip load to be effectively captured by the AR (1) model, resulting in a stationary residual signal a_k with small variance. However, when chatter vibration starts to build up, the local variation caused by the chip regeneration content in x_k is no longer negligible and the RLS algorithm can no longer adapt fast enough to capture the rapid changes in x_k, leading to an a_k with increasing variance. In this case, a standard univariate control chart can be implemented to monitor a_k for chatter detection. Chatter is signaled when the amplitude of a_k exceeds the predetermined control limits. The upper control limit (UCL) and lower control limit (LCL) of the control chart can be set as

$$\text{UCL} = L\sigma, \qquad \text{LCL} = -L\sigma \tag{16}$$

where σ is the standard deviation estimated from a_k during stable cutting and L is a real, positive number determined from the acceptable false alarm rate α (i.e., the probability of issuing an alarm when chatter does not occur). If a_k can be assumed to follow the Gaussian distribution, L can be determined as

$$Z(z \le L) = 1 - \frac{\alpha}{2} \tag{17}$$

where $Z(z)$ stands for the cumulative distribution function of the standard Gaussian distribution. During stable cutting, the expected number of successive samples that fall in the control limits before a false alarm is activated, referred to as the average run length (ARL_0), is given by

$$\text{ARL}_0 = \frac{1}{\alpha} \tag{18}$$

It is clear from the preceding discussion that setting up the control limits for the control chart is independent of any cutting conditions; L is chosen based on the acceptable false alarm rate and σ is estimated from a_k at the very beginning of each cut. Therefore, the proposed chatter detection algorithm is expected to work independently of cutting conditions and the tool/ workpiece materials.

2.2.4 Median Filter. The last step in the chatter detection algorithm is to remove any singular peaks in a_k so that the false alarm rate is reduced. Singular peaks may result from a hard spot in the workpiece, tool breakage or chipping, etc. In these cases, a one tap adaptive filter cannot respond fast enough to the sudden large variation in the force signal and a singular out-of-control point may appear in a_k. It is proposed to use a median filter with a window size of three to remove such singular peaks. The operation of the median filter is described as

$$a_k^M = \text{median}(a_{k-1}, a_k, a_{k+1}) \tag{19}$$

where a_k^M is the signal to be used for chatter detection. Note that the median filter delays chatter detection by one spindle period because a_k^M cannot be determined until a_{k+1} becomes available.

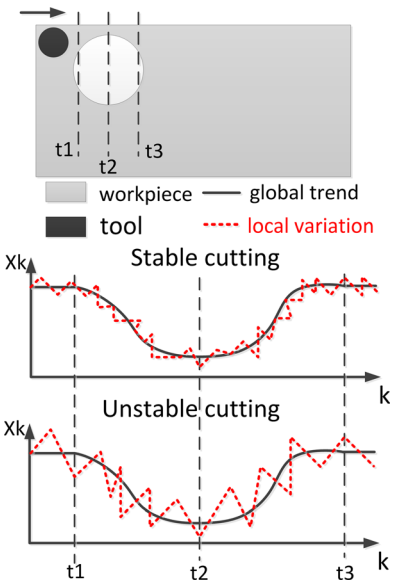

Fig. 3 Global trend and local variation in x_k

2.3 Limitations and Discussion. It has been pointed out in Ref. [3] that chatter frequencies can be integer multiples of the spindle frequency ω when chatter occurs in the form of a flip bifurcation, where the chatter frequencies ω_c are given by

$$\omega_c = \frac{2k+1}{2}\omega_T = \frac{2k+1}{2} z\omega, \qquad k = 0, 1, 2... \tag{20}$$

where z is the number of teeth on the cutting tool. Clearly, for an even number of teeth, the chatter frequencies ω_c are integer multiples of ω, which will be completely removed during the spindle period averaging and adaptive filtering steps. Noticing that ω_c can never be an integer multiple of ω_T, it is proposed to use tooth period averaging on $df(t)^2$ instead of spindle period averaging

$$x_k = \int_{k\tau_T}^{(k+1)\tau_T} df(t)^2 dt \tag{21}$$

While the tooth period averaging approach can potentially detect chatter earlier because a new x_k becomes available every tooth period and a_k^M is checked against the control limits z times per spindle period (instead of once per spindle period in the spindle period averaging approach), tool runout can cause periodic fluctuations

in x_k and a_k^M with a period of z (note that x_k and a_k^M are time series sampled at unit frequency). An additional notch filter at the frequency of $1/z$ is then needed to remove the runout induced periodic fluctuations from x_k, thereby increasing the computational cost. Since flip bifurcation usually occurs in high speed and highly interrupted cutting, the spindle period averaging approach is expected to be more frequently used.

2.4 Dominant Chatter Frequency Estimation. To facilitate chatter suppression, the dominant chatter frequency needs to be estimated from the cutting force signal once the onset of chatter has been recognized by the control chart. The spindle frequency or one of its harmonics is then matched with the estimated dominant chatter frequency to suppress chatter [10]. Transform based methods such as the fast Fourier transform (FFT) may be applied to the cutting force signal collected near the chatter onset point, and the dominant chatter frequency can be identified as the highest peak in the spectrum. However, a tradeoff has to be made between the stationarity assumption (i.e., the signal is approximately stationary near the chatter onset point) and the frequency resolution: the greater the number of data samples, the better the frequency resolution, but the less reasonable the stationarity assumption. Here, a computationally more efficient algorithm that obviates the aforementioned difficulty is proposed.

In the incipient stages of chatter development, the chip regeneration part in the cutting force is still small in magnitude compared to the periodic part. Therefore, the period part needs to be removed from the cutting force signal by applying a first order difference [63]

$$f(t) = \hat{F}(t) - \hat{F}(t-\tau) \tag{22}$$

Note that if flip bifurcation is expected to occur, τ_T instead of τ will show up in Eq. (22) and a notch filter at $1/z$ will be needed to preprocess $f(t)$. After the first order difference, only the chip regeneration content and the stochastic disturbance remain and the Fourier series expansion of $f(t)$ has the following form:

$$f(t) \approx \sum_{k=-N_2}^{N_2} [C_k^+ e^{j(\omega_c + k\omega_T)t} + C_k^- e^{j(-\omega_c - k\omega_T)t}] + v(t) \tag{23}$$

where $v(t)$ is the white noise in $f(t)$. Note that $v(t)$ is different from $w(t)$ in Eq. (8) because of the first order difference in Eq. (22). Let $f(n)$ and $v(n)$ be the discretized versions of $f(t)$ and $v(t)$, respectively, and perform a change of notation on Eq. (23) as follows:

$$f(n) = \sum_{k=1}^{p} A_k e^{j\omega_k n} + v(n) \tag{24}$$

where $p = 4N_2 + 2$ and A_k and ω_k denote the complex amplitude and frequency of the corresponding harmonic, respectively. The estimation of ω_c from $f(n)$ is based on the eigendecomposition of the autocorrelation matrix of $f(n)$, which is defined as

$$R_f = \begin{bmatrix} R_f(0) & R_f(-1) & R_f(-2) & \dots & R_f(-M+1) \\ R_f(1) & R_f(0) & R_f(-1) & \dots & R_f(-M+2) \\ R_f(2) & R_f(1) & R_f(0) & \dots & R_f(-M+3) \\ \dots & \dots & \dots & & \dots \\ R_f(M-1) & R_f(M-2) & R_f(M-3) & \dots & R_f(0) \end{bmatrix} \tag{25}$$

where $R_f(k) = E[f(n)f^*(n-k)]\, R_f(-k) = R_f^*(k)$

It can be shown that if the phases of each harmonic (contained in A_k) are statistically independent from each other, R_f can be decomposed into two parts [62]

$$R_f = \sum_{k=1}^{p} |A_k|^2 e_k e_k^H + \sigma_v^2 I_{M\times M} \tag{26}$$

where

$$e_k = [\,1 \quad e^{-j\omega_k} \quad e^{-j2\omega_k} \quad \dots \quad e^{-j(M-1)\omega_k}\,]^H \tag{27}$$

is known as the signal vector, σ_v^2 is the variance of $v(t)$, and H denotes the Hermitian transpose. The first part in Eq. (26), denoted as R_s, is an $M \times M$ matrix of rank p, while the second part, denoted as R_n, is an identity matrix. Performing an eigendecomposition on each part, we obtain

$$R_f = \sum_{i=1}^{p} \lambda_i^s v_i v_i^H + \sum_{i=1}^{M} \sigma_v^2 v_i v_i^H \tag{28}$$

where $v_1, v_2, \dots, v_M$ is a set of orthonormal eigenvectors for R_s and $\lambda_1^s, \lambda_2^s, \dots, \lambda_p^s$ are the first p nonzero eigenvalues of R_s. The rest of the eigenvalues are zero. Rearranging Eq. (28), we obtain

$$R_f = \sum_{i=1}^{p} (\lambda_i^s + \sigma_v^2) v_i v_i^H + \sum_{i=p+1}^{M} \sigma_v^2 v_i v_i^H \tag{29}$$

The first p eigenvectors in Eq. (29) $v_1, v_2, \dots, v_p$, are referred to as the signal eigenvectors and the last $(M-p)$ eigenvectors $v_{p+1}, v_{p+2}, \dots, v_M$ are referred to as the noise eigenvectors. Since R_f is a Hermitian matrix and the eigenvectors corresponding to different eigenvalues are orthogonal to each other [62], the signal eigenvectors corresponding to eigenvalues $(\lambda_i^s + \sigma_v^2)$ are orthogonal to the noise eigenvectors corresponding to eigenvalues σ_v^2. Accordingly, the space spanned by the signal eigenvectors (known as the signal subspace) is orthogonal to the space spanned by the noise eigenvectors (known as the noise subspace). Since signal vectors e_k also lie in the signal subspace [64], they are orthogonal to any vector v that lies in the noise subspace, or

$$e_k^H v = \sum_{m=0}^{M-1} v(m) e^{-jm\omega_k} = 0, \;\; k = 1, 2, \dots p \tag{30}$$

Equation (30) essentially means that the discrete time Fourier transform of v has p zeros at $\omega_1, \omega_2, \dots, \omega_p$. Or, equivalently, $V(z)$, the z-transform of v, has p zeros on the unit circle in the z-plane, with the phase angle of each zero given by $\omega_k/2\pi$.

Although v can be an arbitrary vector in the noise space, it has been suggested in Ref. [65] to always use the minimum norm vector in the noise subspace, which is given by

$$v_{\min} = \frac{V_n V_n^H u_1}{u_1^H V_n V_n^H u_1} \tag{31}$$

where $V_n = [v_{p+1}\; v_{p+2} \dots\; v_M]$ and $u_1 = [1\; 0 \dots 0]^T$.

The algorithm for determining the dominant chatter frequency among all p complex exponentials in Eq. (24) can now be established as follows:

1. Compute the $M \times M$ autocorrelation matrix R_f, according to Eq. (25). Since R_f is both Hermitian and Toeplitz, only the M independent elements in R_f need to be computed. In practice, the expectation operator E is approximated by the sample average. Note that since $f(n)$ is a time-varying signal, its autocorrelation matrix is also time varying. Therefore, at any time instant the autocorrelation matrix is computed using only the latest N data points. At time n, the estimated time dependent autocorrelation coefficient at lag k, $\hat{R}_f^n(k)$ is computed as

$$\hat{R}_f^n(k) = \frac{1}{N} \sum_{i=n-N+1}^{n} f(i) f^*(i-k) \qquad k = 0, 1, \dots M-1 \tag{32}$$

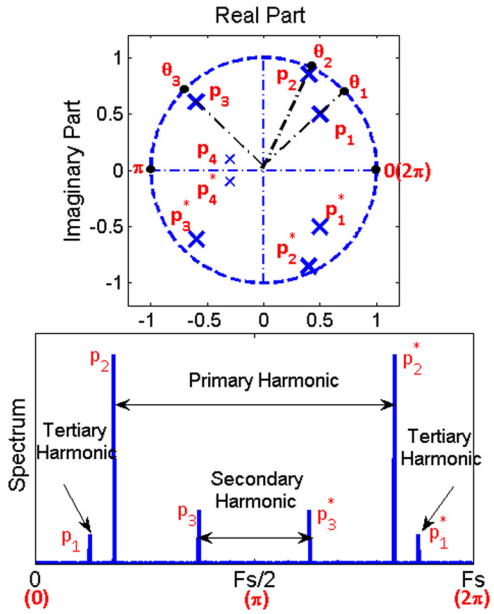

Fig. 4 Relationship between the pole location and the spectrum of the signal

Since only the noise eigenvectors of R_f are of interest, the normalization by N is unnecessary and can be dropped for all elements in R_f

$$\hat{R}_f^n(k) = \sum_{i=n-N+1}^{n} f(i)f^*(i-k) \tag{33}$$

It is straightforward to show that

$$\hat{R}_f^n(k) = \hat{R}_f^{n-1}(k) + f(n)f^*(n-k) - f(n-N)f^*(n-N-k) \tag{34}$$

which provides a way to evaluate the autocorrelation matrix recursively in time.

2. Perform the eigendecomposition on R_f, find its $(M-p)$ noise eigenvectors: $v_{p+1}, v_{p+2}, \ldots, v_M$ and the minimum norm vector $v_{\min}$, according to Eq. (31). Since we are dealing with a real signal $f(n)$, R_f is always real and symmetric, which can significantly reduce the computation complexity when computing its eigenvalues and eigenvectors [64].

3. Compute the roots of the $(M-1)$th order polynomial $V_{\min}(z)$, which is the z-transform of $v_{\min}$. The roots are found by computing the eigenvalues of the companion matrix which is $(M-1)\times(M-1)$ in size.

4. Sort all $(M-1)$ roots obtained in Step 3 to determine the root that is closest to the unit circle in the z-plane (i.e., the root whose magnitude is closest to unity), calculate its phase angle θ (in radians), and determine the dominant chatter frequency ω_c (in rad/s) from it

$$\omega_c = \theta F_s \tag{35}$$

where F_s is the sampling frequency (in Hz).

An example illustrating the relationship between the pole locations in the z-plane and the spectrum of the signal is given in Fig. 4. In the z-plane, the phase angle θ is simply the angle made between the positive direction of the horizontal axis and the line connecting the pole and the center of the unit circle. In this example, $(M-1)=8$. Note that the pair of poles (p_2, p_2^*) closest to the unit circle corresponds to the strongest harmonics in the signal, i.e., the dominant chatter frequency, while the pair of poles close to the center of the unit circle (p_4, p_4^*) has little impact on the spectrum.

Since, in most cases, only the dominant chatter frequency is of interest, it is reasonable to set $p=2$, i.e., it is assumed that there exist only two complex exponentials in $f(n)$: ω_c and $-\omega_c$. The dimension of R_f, M needs to be larger than p.

The chatter detection and chatter frequency estimation algorithm is summarized block-diagrammatically in Fig. 5.

3 Experiments and Results

A set of end milling experiments was performed in order to verify the proposed methodology. The tests were designed such that the tool encounters different types of geometric features (holes with different diameters, slots, curvilinear tool paths, etc.) along the tool path. Cutting force signals were collected using a table-type force dynamometer (Kistler 9257B) at 10 KHz. Since the direction of the tool motion with respect to the workpiece coordinate system may change along the tool path, the source signal is defined as follows to make it as directionally independent as possible:

$$df(t) = \sqrt{\left[\frac{dF_x(t)}{dt}\right]^2 + \left[\frac{dF_y(t)}{dt}\right]^2} \tag{36}$$

3.1 Chatter Detection. The first two tests we examine the capability of the chatter detection algorithm to recognize chatter

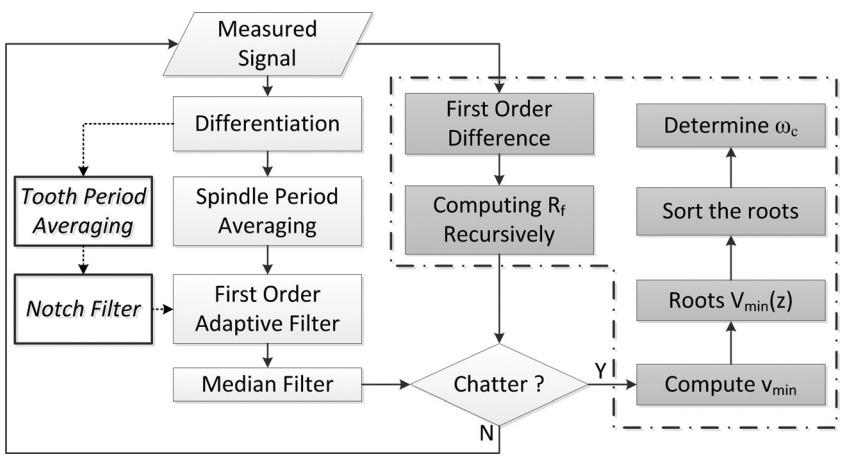

Fig. 5 Flow chart of the chatter detection and chatter frequency estimation method

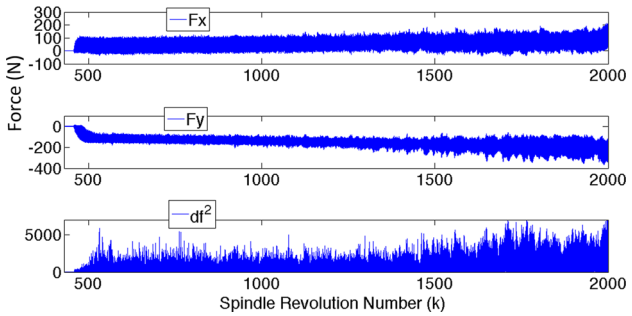

Fig. 6 Inputs and outputs of the chatter detection algorithms for Test 1 (*a*) (four flute 6.35 mm carbide tool, 1018 steel workpiece, 3400 rpm, 0.0254 mm feed/tooth, 50% radial immersion, 2.54 mm depth of cut at beginning)

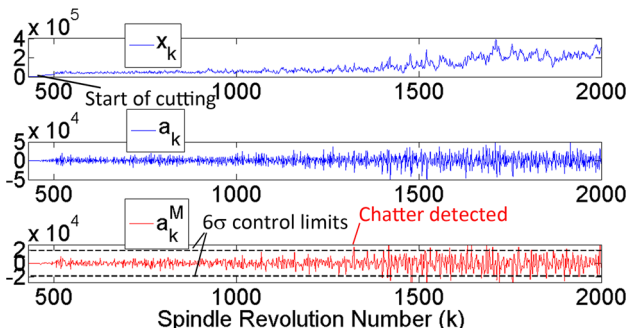

Fig. 7 Inputs and outputs of the chatter detection algorithms for Test 1 (*b*)

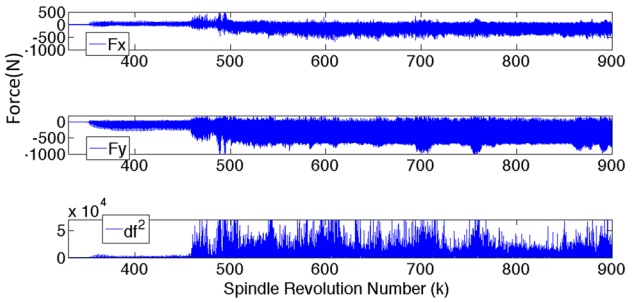

Fig. 8 Inputs and outputs of the chatter detection algorithms for Test 2 (*a*) (two flute 25.4 mm carbide tool, 1018 steel workpiece, 1200 rpm, 0.0381 mm feed/tooth, 25% radial immersion, 2.54 mm axial depth of cut)

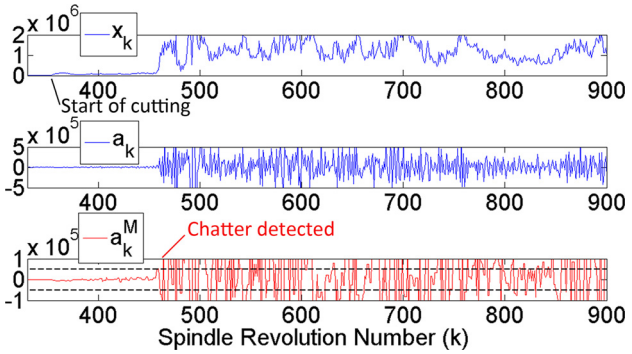

Fig. 9 Inputs and outputs of the chatter detection algorithms for Test 2 (*b*)

when chatter is actually occurring, while the following three tests investigate if the proposed algorithm can distinguish between chatter and workpiece geometry-induced transients in the cutting forces. The control limits in all control charts are set as $L=6$, which corresponds to a false alarm rate (α) of 2×10^{-9} and an ARL_0 of 5×10^8. In other words, only one false alarm is expected after 5×10^8 spindle revolutions, according to the univariate control chart theory.

3.1.1 Test 1. In this test, chatter developed during a linear cut where the axial depth of the cut increased linearly from 2.54 mm. The inputs (the two in-plane cutting forces) and outputs of the four-step chatter detection algorithm are shown in Figs. 6 and 7. A gentle linear trend is observed in F_x and F_y due to the increasing axial immersion. At the beginning of the cut, x_k is characterized by small local variations superimposed on a time varying global trend. The one tap adaptive filter then successfully removes the global trend and leads to the zero-mean residuals a_k and a_k^M. As the chip regeneration part in the cutting force signal gradually builds up, the amplitude of the local variations in x_k also grows, resulting in residuals with increased variance. Eventually, chatter was detected around the 1322th spindle period, about 130 spindle periods earlier than the appearance of chatter marks on the workpiece.

3.1.2 Test 2. In this test, chatter developed during a linear cut with constant axial and radial depths of the cut. The inputs and outcomes of the individual steps in the algorithm are shown in Figs. 8 and 9. It can be seen that in the first 100 spindle revolutions after the start of cutting (~350th spindle revolution), the cutting forces are stable, x_k has a constant DC trend with small local variations and the residuals have very small variance. When chatter starts to build up, large variations appear in x_k, a_k, and a_k^M. Chatter is detected around the 460th spindle period, about 30 spindle periods ahead of the appearance of chatter marks on the workpiece.

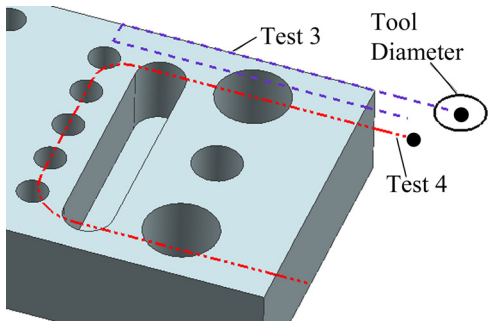

Fig. 10 Workpiece geometries and toolpaths for cutting Tests 3 and 4

In the previous two tests, chatter was successfully recognized by the proposed algorithm ahead of fully developed chatter, i.e., before chatter marks are observed on the workpiece. The workpiece is not damaged when the chatter alarm is issued, which means that corrective measures can still be taken to suppress chatter. The following three cutting tests examine the capability of the proposed algorithm to distinguish between chatter and various types of transients (e.g., tool entry/exit, sudden changes in workpiece geometry). Due to these transients, the cutting force signals become nonstationary and cannot be directly used in chatter detection.

3.1.3 Test 3. The workpiece geometry for this test is illustrated in Fig. 10. The beginning of the tool path is indicated with a black dot. The tool intersects an existing hole on the first leg of the tool path, makes two 90 deg turns, crosses a slot, and temporarily jumps out of cut on the second leg. The cutting force signals shown in Fig. 11 are clearly nonstationary, which leads to a time

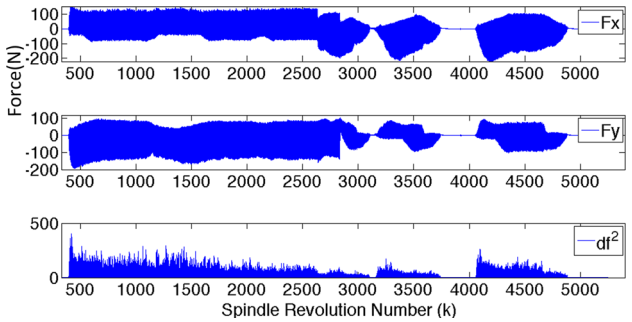

Fig. 11 Inputs and outputs of the chatter detection algorithms for Test 3 (*a*) (two flute 12.7 mm carbide tool, aluminum 7050 workpiece, 2400 rpm, 50%–100% radial immersion, 2.54 mm axial depth of cut, 0.016 mm feed/tooth)

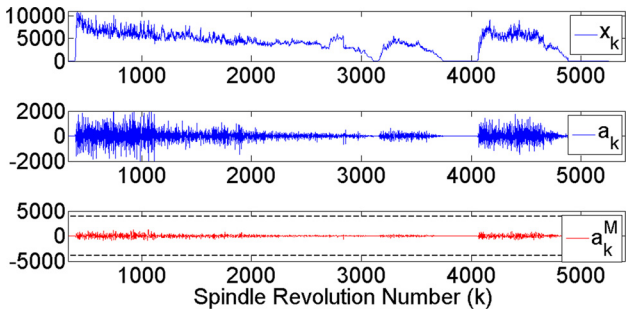

Fig. 12 Inputs and outputs of the chatter detection algorithms for Test 3 (*b*)

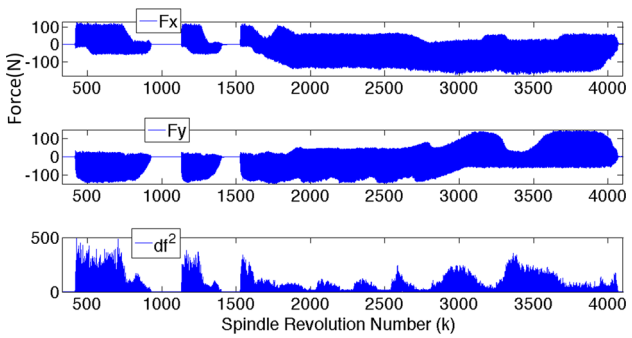

Fig. 13 Inputs and outputs of the chatter detection algorithms for Test 4 (*a*) (two flute 12.7 mm carbide tool, aluminum 7050 workpiece, 2400 rpm, 50%–100% radial immersion, 1.905 mm axial depth of cut, 0.0254 mm feed/tooth)

varying global trend in x_k. The one tap adaptive filter removes the trend in x_k and produces a zero-mean residual a_k^M to be used for chatter detection. No chatter was observed in this test (i.e., no chatter marks), and a_k^M lies within the control limits throughout the cutting test, as shown in Fig. 12.

3.1.4 Test 4. The workpiece geometry for this test is also shown in Fig. 10 and the beginning of the tool path is indicated with a black dot. In this test, the tool intersects a series of existing holes and slots along a curvilinear toolpath. Similar to Test 3, the time-varying trend in x_k due to nonstationary cutting forces are removed by the adaptive filter, resulting in a zero-mean residual signal to be used for chatter prediction (see Fig. 13). No violation of the control limits is observed in Fig. 14, which suggests that no chatter occurred during the cutting operation. This is consistent with observing the workpiece surface.

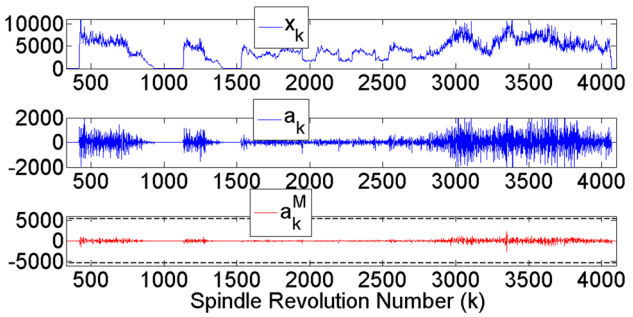

Fig. 14 Inputs and outputs of the chatter detection algorithms for Test 4 (*b*)

Fig. 15 Workpiece geometry and toolpath for cutting Test 5

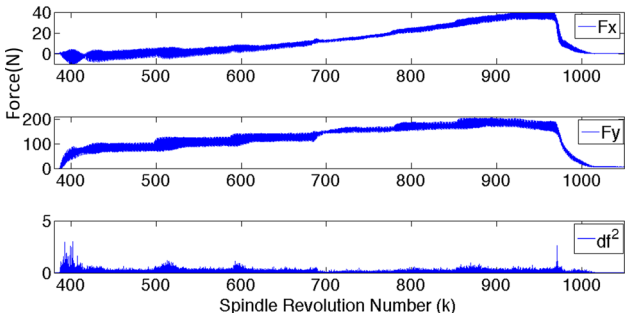

Fig. 16 Inputs and outputs of the chatter detection algorithms for Test 5 (*a*) (four flute 6.35 mm high speed steel tool, aluminum 7050 workpiece, 2400 rpm, 50% radial immersion, 3.81 mm–11.43 mm axial depth of cut, 0.0381 mm feed/tooth)

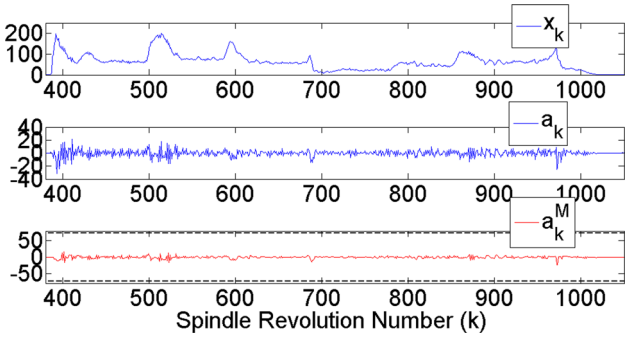

Fig. 17 Inputs and outputs of the chatter detection algorithms for Test 5 (*b*)

3.1.5 Test 5. The workpiece geometry for this test is shown in Fig. 15, where the axial depth of the cut increases in five steps along a straight line. The steps in the axial depth of the cut are also evident in the cutting force signals (see Fig. 16). Again, the time varying trend in x_k due to the time varying chip load is effectively removed, resulting in a zero-mean stationary residual signal

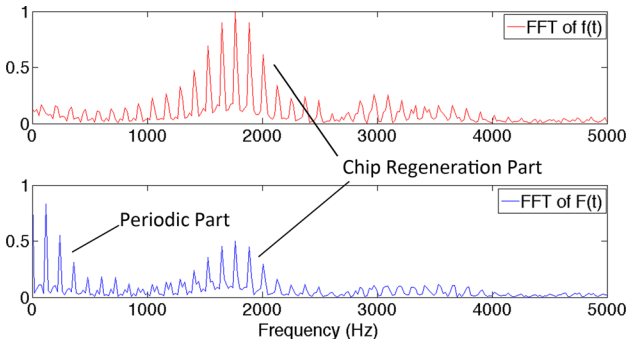

Fig. 18 Comparison of the FFT of *f*(*t*) (top) and *F*(*t*) (bottom)

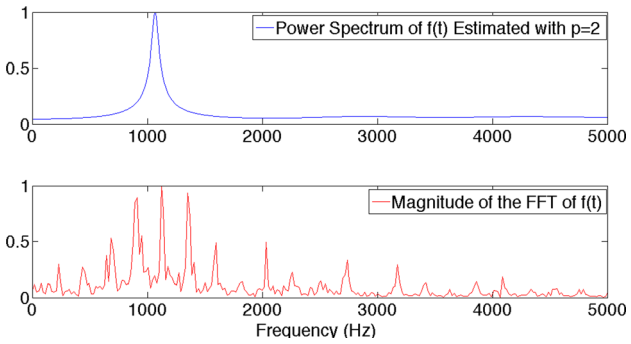

Fig. 19 Dominant chatter frequency estimated by the proposed algorithm (top) and the FFT (bottom) (data is from Test 1)

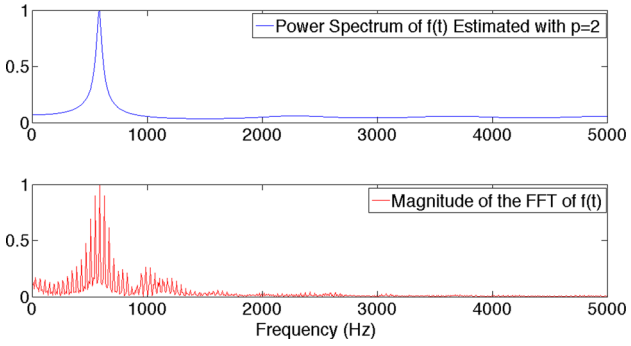

Fig. 20 Dominant chatter frequency estimated by the proposed algorithm (top) and the FFT (bottom) (data is from Test 2)

that lies in the 6σ control limits. No chatter alarm is signaled by the control chart in Fig. 17, which is in agreement with actual observations during the test.

In Tests 3–5, the proposed algorithm successfully reduces the nonstationary cutting force signals into zero-mean residual signals for chatter detection. No false chatter alarm is issued due to geometry-induced transients in the cutting force, which proves that the proposed algorithm is capable of distinguishing between chatter vibrations and transient dynamics due to changing workpiece geometry.

3.2 Chatter Frequency Estimation. The performance of the proposed chatter frequency estimation algorithm is investigated in this section and compared with the FFT. The data used for estimation are the force signals collected during the three spindle revolutions immediately before chatter is signaled by the control chart. It is assumed that during these three spindle periods the cutting force signal is stationary so that the FFT can be computed. For the proposed chatter estimation algorithm $M = 8, p = 2$.

First, the spectra of $F(t)$ and $f(t)$ are compared in Fig. 18. For illustration purposes, all of the FFTs and spectra shown are normalized by their maximum amplitude. In Fig. 18 it can be seen that when chatter is just indicated by the control chart, the amplitude of the chip regeneration content is still small compared to the spindle rotation frequencies in $F(t)$. After a first order difference is performed (as described in Eq. (22)), the spindle rotation frequencies vanish, which facilitates the estimation of the dominant chatter frequency.

The dominant chatter frequencies estimated by the proposed algorithm are compared with the ones estimated using the FFT in Figs. 19 and 20. Note that for the sake of illustration, the spectrum of $f(t)$ estimated using the proposed algorithm is presented and the dominant chatter frequency is identified as a singular peak in the spectrum. In practice, since only the dominant chatter frequency is of interest, it is unnecessary to compute the whole spectrum. In both cases, the chatter frequency estimated using the complex exponentials model agree very well with the highest peak in the corresponding FFTs, which validates the proposed algorithm. It will be shown in the next section that the proposed algorithm is computationally more efficient.

4 Computational Complexity Analysis

The computational cost of the proposed chatter detection algorithm and the dominant chatter frequency estimation algorithm are detailed in Table 1. It is clear that the number of computations needed for the proposed chatter detection algorithm is linear with the number of data available in a spindle period (i.e., the sampling rate). This is comparable with the computational cost of the wavelet transform ($O(N)$) and more efficient than the FFT, which is $O(N \log(N))$.

It is interesting to note that the computational cost of the proposed chatter frequency estimation algorithm is a function of only

Table 1 Computational complexity analysis of the proposed algorithm

	Operations	Computational costs
Chatter detection	Differentiation (Eq. (10))	1 addition[a] per $F(t)$ sample
	Spindle period averaging (Eq. (11))	1 multiplication and addition per $F(t)$ sample
	One tap adaptive filtering (Eq. (15))	6 multiplications, 3 additions and 1 division Per spindle period [62]
	Median filter (Eq. (19))	3 comparisons per spindle period
Chatter frequency estimation	First order difference (Eq. (22))	1 addition per $F(t)$ sample
	Computation of R_f (Eq. (34))	$2M$ additions and multiplications per $F(t)$ sample when implemented recursively in time
	Eigendecomposition of R_f	$\sim M^3$ additions and multiplications
	Computation of v_{min} (Eq. (31))	$M(M-p)$ multiplications, $M(M-p-1)$ additions, and 1 division
	Rooting an $(M-1)$ order polynomial (Eq. (30))	$\sim(M-1)^3$ additions and multiplications
	Determine the dominant chatter frequency (Eq. (35))	$(M-2)$ comparisons, one multiplication

[a]All computations are real.

M, the size of the autocorrelation matrix R_f, and is independent of the data size N. On the contrary, the computational cost of the FFT is a function of the data size N. After chatter is signaled by the control chart, the number of real multiplications needed to arrive at the dominant chatter frequency using the proposed algorithm is approximately $M^3 + (M-1)^3 + M(M-p) + 1$. On the contrary, if a radix-2 FFT is adopted, the number of multiplications needed is approximately $N \log_2(N)$. As long as the following holds:

$$M^3 + (M-1)^3 + (M-p) + 1 < N\log_2(N) \tag{37}$$

the proposed algorithm will have an advantage in computational cost. Since N is typically chosen to be a large number to achieve adequate frequency resolution in the FFT, Eq. (37) is usually true. In addition, if the FFT is used, $(N-1)$ comparisons are needed to locate the peak frequency in the spectrum, while for the proposed algorithm only $(M-2)$ comparisons are needed to sort all the roots. If we select $p=2$, $M=8$ and the number of data to be used for chatter frequency estimation is $N=1024$, the proposed method saves approximately 9336 in the number of multiplications and 1017 in the number of comparisons. The savings in computation buys more time for taking corrective actions to suppress chatter.

Another advantage of the proposed chatter frequency estimation algorithm is the savings in memory usage. For the proposed algorithm, only the $\hat{F}(t)$ sampled in the latest spindle period needs to be stored in memory for computing $f(t)$ and all of the past $f(t)$ are compressed into the M independent elements in R_f. For the FFT, however, not only the $\hat{F}(t)$ in the latest spindle period needs to be saved for computing $f(t)$, but a buffer needs to be allocated in the memory to hold the latest N number of $f(t)$ for chatter frequency estimation.

5 Conclusions

A novel model-based and computationally efficient algorithm for incipient detection of milling chatter and estimation of the dominant chatter frequency based on the cutting force signal is presented and experimentally validated. The proposed method is shown to be capable of detecting chatter and accurately estimating the chatter frequency before chatter is fully developed. It was also found to be capable of distinguishing between chatter and transients in the cutting force caused by changes in workpiece geometry and/or tool entry/exit. The algorithm is cheaper in terms of the computational cost and memory usage than frequency domain transform based methods such as the FFT and can be implemented in low cost microcontrollers for on-line detection and suppression of chatter. Although the method is derived based on cutting force models, the intimate relationship between force and other types of signals suggests that it may also be applied to cutting torque and acceleration signals. The cutting torque signal is of special interest because of its directional independence with respect to tool movement. Future work will include evaluating the performance of the algorithm with tool direction-independent signals and under different cutting conditions.

Acknowledgment

This research was supported by Boeing Research and Technology.

References

[1] Altintas, Y., Stepan, G., Merdol, D., and Dombovari, Z., 2008, "Chatter Stability of Milling in Frequency and Discrete Time Domain," CIRP J. Manuf. Sci. Technol., **1**(1), pp. 35–44.
[2] Budak, E., and Altintas, Y., 1998, "Analytical Prediction of Chatter Stability in Milling—Part I: General Formulation," ASME J. Dyn. Sys., Meas., Control, **120**(1), pp. 22–30.
[3] Insperger, T., and Stepan, G., 2004, "Vibration Frequencies in High-Speed Milling Processes or a Positive Answer to Davies, Pratt, Dutterer and Burns," ASME J. Manuf. Sci. Eng., **126**(3), pp. 481–487.
[4] Insperger, T., Stépán, G., Bayly, P. V., and Mann, B. P., 2003, "Multiple Chatter Frequencies in Milling Processes," J. Sound Vib., **262**(2), pp. 333–345.
[5] Davies, M. A., Pratt, J. R., Dutterer, B., and Burns, T. J., 2002, "Stability Prediction for Low Radial Immersion Milling," ASME J. Manuf. Sci. Eng., **124**(2), pp. 217–225.
[6] Stepan, G., Dombovari, Z., and Muñoa, J., 2011, "Identification of Cutting Force Characteristics Based on Chatter Experiments," CIRP Ann., **60**(1), pp. 113–116.
[7] Braun, S., 1975, "Signal Processing for the Determination of Chatter Threshold," CIRP Ann., **24**(1), pp. 315–320.
[8] Kuljanic, E., Sortino, M., and Totis, G., 2008, "Multisensor Approaches for Chatter Detection in Milling," J. Sound Vib., **312**, pp. 672–693.
[9] Delio, T., Tlusty, J., and Smith, S., 1992, "Use of Audio Signals for Chatter Detection and Control," ASME J. Eng. Industry, **114**(2), pp. 146–157.
[10] Smith, S., and Delio, T., 1992, "Sensor-Based Chatter Detection and Avoidance by Spindle Speed Selection," ASME J. Dyn. Sys., Meas., Control, **114**(3), pp. 486–492.
[11] Smith, S., and Tlusty, J., 1992, "Stabilizing Chatter by Automatic Spindle Speed Regulation," CIRP Ann., **41**(1), pp. 433–436.
[12] Kondo, E., Ota, H., and Kawai, T., 1997, "A New Method to Detect Regenerative Chatter Using Spectral Analysis, Part 1: Basic Study on Criteria for Detection of Chatter," ASME J. Manuf. Sci. Eng., **119**(4A), pp. 461–466.
[13] Tangjitsitcharoen, S., 2009, "In-Process Monitoring and Detection of Chip Formation and Chatter for CNC Turning," J. Mater. Process. Technol., **209**, pp. 4682–4688.
[14] Tlusty, J., and Ismail, F., 1983, "Special Aspects of Chatter in Milling," ASME J. Vib. Acoust., **105**(1), pp. 24–32.
[15] Altintas, Y., and Chan, P. K., 1992, "In-Process Detection and Suppression of Chatter in Milling," Int. J. Mach. Tools Manuf., **32**(3), pp. 329–347.
[16] Rahman, M., 1988, "In-Process Detection of Chatter Threshold," ASME J. Eng. Industry, **110**(1), pp. 44–50.
[17] Ding, S., Izamshah, R. A. R., Mo, J., and Zhu, Y., 2011, "Chatter Detection in High Speed Machining of Titanium Alloys," Key Eng. Mater., **458**, pp. 289–294.
[18] Weck, M., Verhaag, E., and Gathier, M., 1975, "Adaptive Control for Face Milling Operations With Strategies for Avoiding Chatter Vibrations and Automatic Cut Distribution," CIRP Ann., **24**(1), pp. 405–409.
[19] Kakinuma, Y., Sudo, Y., and Aoyama, T., 2011, "Detection of Chatter Vibration in End Milling Applying Disturbance Observer," CIRP Ann., **60**(1), pp. 109–112.
[20] Choi, T., and Shin, Y. C., 2003, "On-Line Chatter Detection Using Wavelet-Based Parameter Estimation," ASME J. Manuf. Sci. Eng., **125**(1), pp. 21–28.
[21] Berger, B. S., Minis, I., Harley, J., Rokni, M., and Papadopoulos, M., 1998, "Wavelet Based Cutting State Identification," J. Sound Vib., **213**(5), pp. 813–827.
[22] Yao, Z., Mei, D., and Chen, Z., 2010, "On-Line Chatter Detection and Identification Based on Wavelet and Support Vector Machine," J. Mater. Process. Technol., **201**(5), pp. 713–719.
[23] Wang, L., and Liang, M., 2009, "Chatter Detection Based on Probability Distribution of Wavelet Modulus Maxima," Rob. Comput.-Integr. Manufact., **25**, pp. 989–998.
[24] Yoon, M. C., and Chin, D. H., 2005, "Cutting Force Monitoring in the Endmilling Operation for Chatter Detection," Proc. Inst. Mech. Eng., Part B, **219**, pp. 455–465.
[25] Abu-Zahra, N. H., and Lange, J. H., 2002, "Tool Chatter Monitoring in Turning Operations Using Wavelet Analysis of Ultrasound Waves," Int. J. Adv. Manuf. Technol., **20**(4), pp. 248–254.
[26] González-Brambila, O., Rubio, E., Jáuregui, J. C., and Herrera-Ruiz, G., 2006, "Chattering Detection in Cylindrical Grinding Processes Using the Wavelet Transform," Int. J. Mach. Tools Manuf., **46**(15), pp. 1934–1938.
[27] Bickraj, K., Kaya, B., Yapici, A., Li, M., Tansel, I. N., and Ozcelik, B., 2007, "Inspection of Chatter Damage in End Milling Operations by Using Wavelet Transformations," Tampico, México, pp. 1–6.
[28] Al-Regib, E., and Ni, J., 2010, "Chatter Detection in Machining Using Nonlinear Energy Operator," ASME J. Dyn. Sys., Meas., Control, **132**(3), p. 034502.
[29] Mitsuishi, M., Nagao, T., Hatamura, Y., and Warisawa, S., 1992, "Real-Time Machining State Detection Using Multiaxis Force Sensing," CIRP Ann., **41**(1), pp. 505–508.
[30] Gradisek, J., Govekar, E., and Grabec, I., 1998, "Time Series Analysis in Metal Cutting Chatter Versus Chatter-Free Cutting," Mech. Syst. Signal Process., **12**(6), pp. 839–854.
[31] Grabec, I., Gradisek, J., and Govekar, E., 1999, "A New Method for Chatter Detection in Turning," CIRP Ann., **48**(1), pp. 29–32.
[32] Berger, B. S., Minis, I., Rokni, M., Papadopoulos, M., Deng, K., and Chavalli, A., 1997, "Cutting State Identification," J. Sound Vib., **200**(1), pp. 15–29.
[33] Messaoud, A., and Weihs, C., 2009, "Monitoring a Deep Hole Drilling Process by Nonlinear Time Series Modeling," J. Sound Vib., **321**(3–5), pp. 620–630.
[34] Du, R., Elbestawi, M. A., and Ullagaddi, B. C., 1992, "Chatter Detection in Milling Based on the Probability Distribution of Cutting Force Signal," Mech. Syst. Signal Process., **6**(4), pp. 345–362.
[35] Schmitz, T. L., 2003, "Chatter Recognition by a Statistical Evaluation of the Synchronously Sampled Audio Signal," J. Sound Vib., **262**(3), pp. 721–730.
[36] Bao, S., Zhang, W., Yu, J., Qiao, S., and Yang, F., 1994, "A New Approach to the Early Prediction of Turning Chatter," ASME J. Vib. Acoust., **116**(4), pp. 485–488.
[37] Berger, B., Belai, C., and Anand, D., 2003, "Chatter Identification With Mutual Information," J. Sound Vib., **267**(1), pp. 178–186.
[38] Berger, B. S., Manzari, J. A., Anand, D. K., and Belai, C., 2001, "Auto-Regressive SVD Algorithms and Cutting State Identification," J. Sound Vib., **248**(2), pp. 351–370.

[39] Pongsathornwiwat, N., and Tangjitsitcharoen, S., 2010, "Intelligent Monitoring and Detection of Chatter in Ball-End Milling Process on CNC Machining Center," 40th International Conference on Computers and Industrial Engineering (CIE), pp. 1–6.
[40] Soliman, E., and Ismail, F., 1997, "Chatter Detection by Monitoring Spindle Drive Current," Int. J. Adv. Manuf. Technol., **13**(1), pp. 27–34.
[41] Messaoud, A., Weihs, C., and Hering, F., 2007, "Detection of Chatter Vibration in a Drilling Process Using Multivariate Control Charts," Comput. Stat. Data Anal., **52**, pp. 3208–3219.
[42] Govekar, E., Gradisek, J., and Grabec, I., 2000, "Analysis of Acoustic Emission Signals and Monitoring of Machining Processes," Ultrasonics, **38**(1–8), pp. 598–603.
[43] Eman, K., and Wu, S. M., 1980, "A Feasibility Study of On-Line Identification of Chatter in Turning Operations," ASME J. Eng. Industry, **102**(4), pp. 315–321.
[44] Faassen, R. P. H., Doppenberg, E. J. J., van de Wouw, N., Oosterling, J. A. J., and Nijmeijer, H., 2006, "Online Detection of the Onset and Occurrence of Machine Tool Chatter in the Milling Process," CIRP 2nd International Conference on High Performance Cutting, Vancouver, Canada.
[45] Li, X. Q., Wong, Y. S., and Nee, A. Y. C., 1997, "Tool Wear and Chatter Detection Using the Coherence Function of Two Crossed Accelerations," Int. J. Mach.Tools Manuf., **37**(4), pp. 425–435.
[46] van Dijk, N. J. M., Doppenberg, E. J. J., Faassen, R. P. H., van de Wouw, N., Oosterling, J. A. J., and Nijmeijer, H., 2010, "Automatic In-Process Chatter Avoidance in the High-Speed Milling Process," ASME J. Dyn. Sys., Meas., Control, **132**(3), p. 031006.
[47] Cho, D. W., and Eman, K. F., 1988, "Pattern Recognition for On-Line Chatter Detection," Mech. Syst. Signal Process., **2**(3), pp. 279–290.
[48] Tarng, Y. S., Li, T. C., and Chen, M. C., 1994, "On-Line Drilling Chatter Recognition and Avoidance Using an ART2—A Neural Network," Int. J. Mach. Tools Manuf., **34**(7), pp. 949–957.
[49] Li, X. Q., Wong, Y. S., and Nee, A. Y. C., 1998, "A Comprehensive Identification of Tool Failure and Chatter Using a Parallel Multi-ART2 Neural Network," ASME J. Manuf. Sci. Eng., **120**(2), pp. 433–442.
[50] Kuljanic, E., Totis, G., and Sortino, M., 2009, "Development of an Intelligent Multisensor Chatter Detection System in Milling," Mech. Syst. Signal Process., **23**(5), pp. 1704–1718.
[51] Tansel, I. N., Wagiman, A., and Tziranis, A., 1991, "Recognition of Chatter With Neural Networks," Int. J. Mach. Tools Manuf., **31**(4), pp. 539–552.
[52] Tarng, Y. S., and Li, T. C., 1995, "Adaptive Pattern Recognition of Drilling Chatter," J. Mater. Process. Technol., **48**(1–4), pp. 247–253.
[53] Wang, M., and Fei, R., 2001, "On-Line Chatter Detection and Control in Boring Based on an Electrorheological Fluid," Mechatronics, **11**(7), pp. 779–792.
[54] Kwak, J. S., and Ha, M. K., 2004, "Intelligent Diagnostic Technique of Machining State for Grinding," Int. J. Adv.Manuf. Technol., **23**(5), pp. 436–443.
[55] Bediaga, I., Muñoa, J., Hernández, J., and López de Lacalle, L. N., 2009, "An Automatic Spindle Speed Selection Strategy to Obtain Stability in High-Speed Milling," Int. J. Mach. Tools Manuf., **49**(5), pp. 384–394.
[56] Mei, D. Q., Li, X., and Chen, Z. C., 2007, "Prediction of Cutting Chatter Based on Hidden Markov Model," Key Eng. Mater., **353–358**, pp. 2712–2715.
[57] Jiang, Y. T., and Zhang, C. L., 2006, "Hybrid HMM/SVM Method for Predicting Cutting Chatter," Proc. SPIE, **6280**, p. 62801Q.
[58] Tansel, I. N., Li, M., Demetgul, M., Bickraj, K., Kaya, B., and Ozcelik, B., 2012, "Detecting Chatter and Estimating Wear From the Torque of End Milling Signals by Using Index Based Reasoner (IBR)," Int. J. Adv. Manuf. Technol., **58**(1–4), pp. 109–118.
[59] Nair, U., Krishna, B. M., and Namboothiri, V. N. N., 2010, "Permutation Entropy Based Real-Time Chatter Detection Using Audio Signal in Turning Process," Int. J. Adv. Manuf. Technol., **46**, pp. 61–68.
[60] Oppenheim, A. V., Schafer, R. W., and Buck, J. R., 1999, *Discrete-Time Signal Processing, Discrete-Time Signal Processing*, Prentice Hall, Upper Saddle River, NJ.
[61] Altintas, Y., 1988, "In-Process Detection of Tool Breakages Using Time Series Monitoring of Cutting Forces," Int. J. Mach. Tools Manuf., **28**(2), pp. 157–172.
[62] Hayes, M. H., 1996, *Statistical Digital Signal Processing and Modeling*, John Wiley and Sons, New York.
[63] Altintas, Y., 2000, *Manufacturing Automation*, Cambridge University Press, Cambridge, England.
[64] Moon, T. K., and Stirling, W. C., 2000, *Mathematical Methods and Algorithms for Signal Processing*, Prentice Hall, Upper Saddle River, NJ.
[65] Kumaresan, R., and Tufts, D. W., 1983, "Estimating the Angles of Arrival of Multiple Plane Waves," IEEE Trans. Aerosp. Electron. Syst., **AES–19**(1), pp. 134–139.